International Journal of Heat and Mass Transfer 61 (2013) 397–408

Contents lists available at SciVerse ScienceDirect

International Journal of Heat and Mass Transfer

journal homepage: www.elsevier.com/locate/ijhmt

Effects of material properties on heating processes in two-layered porous media subjected to microwave energy

Santiphong Klayborworn [1], Watit Pakdee *, Phadungsak Rattanadecho [2], Somsak Vongpradubchai [3]

Research Center of Microwave Utilization in Engineering (R.C.M.E.), Department of Mechanical Engineering, Thammasat University, Klong Luang, Pathumthani, Thailand

ARTICLE INFO

Article history:
Received 12 October 2012
Received in revised form 7 February 2013
Accepted 7 February 2013
Available online 5 March 2013

Keywords:
Microwave heating
Variable-porosity
Natural convection
Saturated porous media
Material properties
Rectangular waveguide

ABSTRACT

Microwave heating of double-layer porous medium is numerically investigated using a proposed numerical model. A two-dimensional domain composed of two porous layers is considered. The two porous layers have different particle sizes, porosities, thermal and dielectric properties. The generalized non-Darcian model developed takes into account of the presence of a solid drag and the inertial effect. The transient Maxwell's equations are solved by using the finite difference time domain (FDTD) method to describe the electromagnetic field in the waveguide and in the media. The temperature profile and velocity field within the media are determined by solution of the momentum and energy equations given by the SIMPLE (Semi-Implicit Method for Pressure Linked Equations) algorithm. This study focuses on effects of diameter, porosity, position and types of particles that have different thermal and dielectric properties. The computed results agree well with the experimental results. While the particle size and porosity mainly affect fluid flow within porous media, the thermal and dielectric properties strongly influence heat transfer mechanism in each layer of porous media.

1. Introduction

Microwave heating of a porous medium is widely implemented in industries, such as heating food, ceramics, biomaterials, concrete manufacture, etc., since microwave energy has many advantages such as short time process, high thermal efficiency, environmentally friendly credentials and high product quality. Microwave radiation penetrates into a material and heats it by a dipolar polarization that occurs millions times per second.

A number of previous works have focused on the drying of unsaturated porous media in which heat and mass transfers were modeled [1–6] however most of these dealt with solid materials and focused on heat conduction within a medium. Some works studied a natural convection induced by microwave heating of fluids, since a complex distribution of electromagnetic waves is shown to be a complicate effect on flow field [7–11]. The effects of natural convection and dielectric properties on liquid layers were studied numerically and experimentally. The heating kinetics strongly depended on the dielectric properties [7]. Natural convection due to buoyancy force strongly affects flow patterns within the water layer during the microwave heating process, and clearly enhances temperature distribution in the layer [8]. Recently, Chaum et al. [8] experimentally investigated the heating process within a packed bed filled with glass beads and water and found that the location of the sample relative to that of heat source had an important effect on the pattern of heating. Other recent works focused on microwave driven convection in pure liquids [9–11]. While the previous studies were based on pure liquids, we pay attention to heating induced by microwave energy in a fluid-saturated porous medium with two layers. One of the apparent applications for microwave heating of fluid-saturated porous medium involves food sterilization or pasteurization [12].

Furthermore, all the previous investigations referred did not account for the effect of variable porosity in the vicinity of the impermeable wall. A region of higher porosity near the wall forms due to the packing of the porous spheres near the column wall is not as efficient as that away from the wall towards the column center [13]. Benenati and Brosilow [14] found a distinct porosity variation with a high porosity region close to the wall in packed beds. Values of porosity those are high close to an impermeable wall decrease to an asymptotic value at about four to five sphere diameters away

* Corresponding author. Address: Department of Mechanical Engineering, Thammasat University (Rangsit Campus), 99 Paholyotin Rd., Klong Luang, Pathumthani 12120, Thailand. Tel.: +66 11 662 5643001–9x3143; fax: +66 11 662 5643023.

E-mail addresses: freshgear@gmail.com (S. Klayborworn), pwatit@engr.tu.ac.th (W. Pakdee), ratphadu@engr.tu.ac.th (P. Rattanadecho), vsomsak@engr.tu.ac.th (S. Vongpradubchai).

[1] Address: 97/3 M.4, T. Tharahat, A. Mueang, Suphanburi 72000, Thailand. Tel.: +66 (0) 81857 9150.

[2] Address: Department of Mechanical Engineering, Thammasat University (Rangsit Campus), 99 Paholyotin Rd., Klong Luang, Pathumthani 12120, Thailand. Tel.: +66 11 662 5643001–5x3153; fax: +66 11 662 5643023.

[3] Address: Department of Mechanical Engineering, Thammasat University (Rangsit Campus), 99 Paholyotin Rd., Klong Luang, Pathumthani 12120, Thailand. Tel.: +66 11 662 5643001–5x3264; fax: +66 11 662 5643023.

0017-9310/$ - see front matter © 2013 Elsevier Ltd. All rights reserved.
http://dx.doi.org/10.1016/j.ijheatmasstransfer.2013.02.020

Nomenclature

C_p	specific heat capacity (J/(kg K))
E	electric fields intensity (V/m)
f	frequency of incident wave (Hz)
g	gravitational constant (m/s^2)
H	magnetic field intensity (A/m)
P	power (W)
p	pressure (Pa)
Q	local electromagnetic heat generation term (W/m^3)
s	Poynting vector (W/m^2)
T	temperature (°C)
t	time (s)
$\tan\delta$	dielectric loss coefficient (–)
u,w	velocity component (m/s)
Z_H	wave impedance (Ω)
Z_l	intrinsic impedance (Ω)

Greek letters

ϕ	porosity (m^3/m^3)
α	thermal diffusivity (m^2/s)
β	coefficient of thermal expansion (1/K)
η	absolute viscosity (Pa s)
ε	permittivity (F/m)
ε'	dielectric constant (F/m)
ε''	dielectric loss factor (F/m)
λ	wavelength (m)
μ	magnetic permeability (H/m)
υ	velocity of propagation (m/s)
ν	kinematics viscosity (m^2/s)
ρ	density (kg/m^3)
σ	electric conductivity (S/m)
ω	angular frequency (rad/s)
ξ	surface tension (N/m)

Subscripts

0	free space
∞	ambient condition
a	air
f	fluid
j	layer number
in	input
p	particle
r	relative

from it [15,16]. Many researchers found that the variation of porosity might significantly affect flow patterns as well as heat transfer features [14,17–19]. The porosity of the bed exhibits sinusoidally damping decay especially at locations near wall [14]. This phenomenon leads to the channeling effect that could significantly modify flow patterns [15,20–22]. Hsiao et al. [18] reported that including the effects of variable porosity and thermal dispersion on natural convection in the region of the heated horizontal cylinder in an enclosed porous medium increased the average Nusselt number and reduced the error between the experimental data and their solutions. Thus, the effects of porosity variation should be taken into account in practice [17,23–25]. For works related to the two-layered porosity medium, Rattanadecho et al. [4] studied influence of time input energy for the microwave on particle size and initial moisture content. It is found that the capillary pressure increases when particle size is smaller and the rate of drying is faster. Prommas et al. [26] showed that the proportion of the benefits of energy and efficiency of exergy depended on the size of the particles, the hydrodynamic properties and the structure of the porous layer. Pakdee and Rattanadecho [27] proposed a mathematical model for the microwave heating of the saturated porous medium with variation-porosity based on distance from the wall of the packed bed. Effects of the size of the particles and the average porosity on the temperature and water flow profile were examined. Numerical results were reliable when compared with values obtained from experiments using a rectangular waveguide for the TE_{10} mode. Recently, effects of electromagnetic field on forced convection in porous media were investigated [28]. The energy separation between solid and fluid phases was modeled using local thermal non equilibrium (LNTE). The results showed that errors stem from assuming local thermal equilibrium the calculation is increased when the Darcy number or power of electromagnetic field or ratio of the thermal diffusivity of solid to fluid increases.

Most previous research studied heating processes in a uniform porosity medium due to microwave heating. Only few studies were interested in microwave heating in a multi-layered medium although microwave heating in a multi-layered saturated materials have been found in broad applications in food applications and hyperthermia system for the treatment of tumor [29,30]. Moreover, no work focusing on effects of material properties have been reported. Therefore, our study aimed to investigate effects of microwave on particle size, porosity and medium properties of particles including thermal and dielectric properties on heating process in two-layered porous materials. The present work particularly includes comparisons between the theoretical analysis, mathematical modeling and experimental results.

2. Experimental setup

Fig. 1 shows the experiment apparatus for microwave heating of a saturated porous medium using a rectangular waveguide. Actual image of the apparatus is shown in Fig. 1(a). The microwave system is a monochromatic wave of TE_{10} mode operating at a frequency of 2.45 GHz. Microwave power used is 300 W. From Fig. 1(b), magnetron (No. 1) generates microwaves and transmits them along the z-direction of the rectangular waveguide (No. 5) with inside cross-sectional dimensions of 109.2×54.61 mm^2 that refers to a testing area (red circle) and a water load (No. 8) that is situated at the end of the wave guide. On the upstream side of the sample, an isolator is used to trap any microwaves reflected from the sample to prevent damage to the magnetron. The powers of incident, reflected and transmitted waves are measured by a wattmeter using a directional coupler (No. 6) (MICRO DENSHI., model DR-5000). Fiberoptic probes (No. 7) (LUXTRON Fluroptic Thermometer (model 790, accurate to ±0.5°C) is employed for temperature measurement. The probes are inserted into the sample, positioned on the XZ plane at $Y = 25$ mm. (see in Fig. 2). Due to the symmetry, temperatures are only measured on one side of the plane. The samples are saturated porous packed beds composed of glass beads and water. The container, with a thickness of 0.75 mm, is made of polypropylene which does not absorb microwave energy.

In our present experiment, the two-layer medium is examined. The glass beads of 0.15 mm and put on top of the glass beads of 0.4 mm in diameter is examined. The averaged (free stream) porosity of the packed bed corresponds to 0.385 and 0.371, respectively.

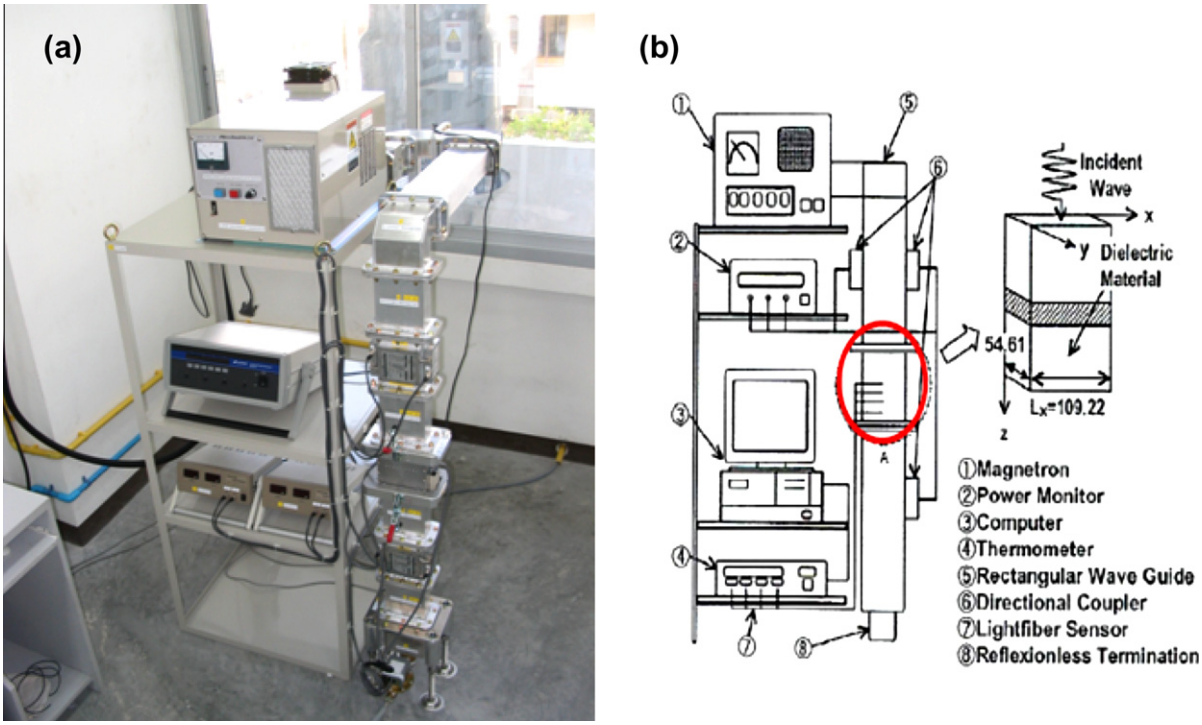

Fig. 1. The microwave heating system with a rectangular waveguide.

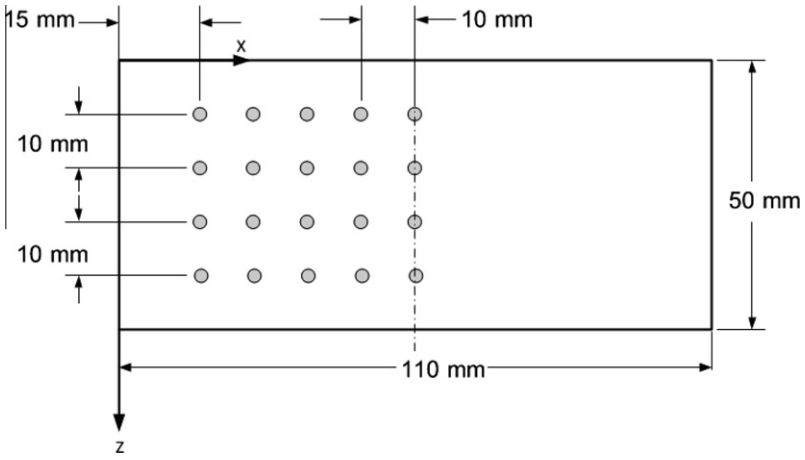

Fig. 2. Locations of temperature measurement in symmetrical *xz* plane.

3. Mathematical formulation

3.1. Analysis of electromagnetic field

Electromagnetic waves are formed with a combination of electric waves and magnetic waves. The magnetic and electric fields of an electromagnetic wave are perpendicular to each other and to the direction of the wave. Microwave is a part of an electromagnetic spectrum that has a particular range of wavelengths. Since the electromagnetic field that is investigated is the microwave field in the TE_{10} mode there is no variation of field in the direction between the broad faces of the rectangular waveguide and it is uniform in the *y*-direction. Consequently, it is assumed that a two dimension heat transfer model in *x* and *z* directions will be sufficient to identify the microwave heating phenomena in a rectangular waveguide [7]. Further assumptions are as follows:

(1) The absorption of microwaves by air in a rectangular wave guide is negligible.
(2) The walls of a rectangular wave guide are perfect conductors.
(3) The effect of the sample container on the electromagnetic and temperature fields can be neglected.

The proposed model is considered in the TE_{10} mode so the Maxwell's equations can be written in term of the electric and magnetic intensities;

$$\varepsilon\frac{\partial E_y}{\partial t}=\frac{\partial H_x}{\partial z}-\frac{\partial H_z}{\partial x}-\sigma E_y \tag{1}$$

$$\mu\frac{\partial H_z}{\partial t}=-\frac{\partial E_y}{\partial x} \tag{2}$$

$$\mu\frac{\partial H_x}{\partial t}=\frac{\partial E_y}{\partial z} \tag{3}$$

where *E* and *H* denote electric field intensity and magnetic field intensity, respectively. Subscripts *x*, *y* and *z* represent the *x*, *y* and

z components of vectors, respectively. Finally, ε is the electrical permittivity, σ is the electrical conductivity and μ is the magnetic permeability. These variables can be defined as follows:

$$\varepsilon = \varepsilon_0 \varepsilon_r \tag{4}$$

$$\mu = \mu_0 \mu_r \tag{5}$$

$$\sigma = 2\pi f \varepsilon \tan\delta, \tag{6}$$

The dielectric properties of porous material depend on temperature in which fractions of fluid and solid are considered based on porosity, ϕ as follows [25]:

$$\varepsilon_r(T) = \varepsilon_r'(T) - j\varepsilon_r''(T) \tag{7}$$

where

$$\varepsilon_r'(T) = \phi\varepsilon_{rf}'(T) + (1-\phi)\varepsilon_{rp}' \tag{8}$$

$$\varepsilon_r''(T) = \phi\varepsilon_{rf}''(T) + (1-\phi)\varepsilon_{rp}'' \tag{9}$$

where ε' and ε'' represent the dielectric constant and the dielectric loss, respectively.

The loss tangent coefficient can be written as:

$$\tan\delta(T) = \frac{\varepsilon_r''(T)}{\varepsilon_r'(T)} \tag{10}$$

When the material is heated unilaterally, it is found that as the dielectric constant and loss tangent coefficient vary, the penetration depth and the electric field within the dielectric material varies. Penetration dept is a measure of how deep the electromagnetic radiation can penetrate into a material. A number of factors can influence penetration depth including properties of the material, intensity and frequency of the electromagnetic wave. The penetration depth is used to denote the depth at which the power density has decreased to 37% of its initial value at the surface [6].

$$D_P = \frac{1}{\frac{2\pi f}{\upsilon}\sqrt{\frac{\varepsilon_r'\left(\sqrt{1+\left(\frac{\varepsilon_r''}{\varepsilon_r'}\right)^2}-1\right)}{2}}} = \frac{1}{\frac{2\pi f}{\upsilon}\sqrt{\frac{\varepsilon_r'\left(\sqrt{1+(\tan\delta)^2}-1\right)}{2}}} \tag{11}$$

where D_p is the penetration depth, ε_r'' is the relative dielectric loss factor and υ is the microwave speed. The penetration depth of the microwave power is calculated according to Eq. (11), which demonstrates how it depends on the dielectric properties of the material. It is noted that products of huge dimensions and with high loss factors may occasionally overheat a considerably thick layer of the outer surface. To prevent such a phenomenon the power density must be chosen so that enough time is provided for the essential heat transfer between boundary and core. If the thickness of the material is less than the penetration depth only a fraction of the supplied energy will become absorbed. For example, the dielectric properties of water show that water moderately dissipate electromagnetic energy into heat. This characteristic depends on the temperature. The water layer at low temperature typically shows slightly greater potential for absorbing microwaves. In the other words, an increase in the temperature typically decreases ε_r'', accompanied by a slight increase in D_p.

The boundary conditions for the TE_{10} mode can be formulated as follows:

(1) Perfectly conducting boundary. Boundary conditions on the inner wall surface of waveguide are given by Faraday's law and Gauss's theorem:

$$E_t = 0, \quad H_n = 0 \tag{12}$$

where subscripts t and n denote the components of tangential and normal directions, respectively.

(2) Continuity boundary condition. Boundary conditions along the interface between sample and air are given by Ampere's law and Gauss's theorem:

$$E_t = E_t', \quad H_t = H_t' \tag{13}$$

(3) The first order absorbing boundary condition applied at both ends of rectangular waveguide:

$$\frac{\partial E_y}{\partial t} = \pm\upsilon\frac{\partial E_y}{\partial z} \tag{14}$$

where ± is represented forward and backward direction and υ is velocity of wave.

(4) The incident wave due to magnetron is given by [7] showing an oscillation of the electric and magnetic intensities by the magnetron:

$$E_y = E_{yin}\sin\left(\frac{\pi x}{L_x}\right)\sin(2\pi f t) \tag{15}$$

$$H_x = \frac{E_{yin}}{Z_H}\sin\left(\frac{\pi x}{L_x}\right)\sin(2\pi f t) \tag{16}$$

where E_{yin} is the input value of electric field intensity, L_x is the length of the rectangular wave guide in the x-direction and Z_H is the wave impedance defined as

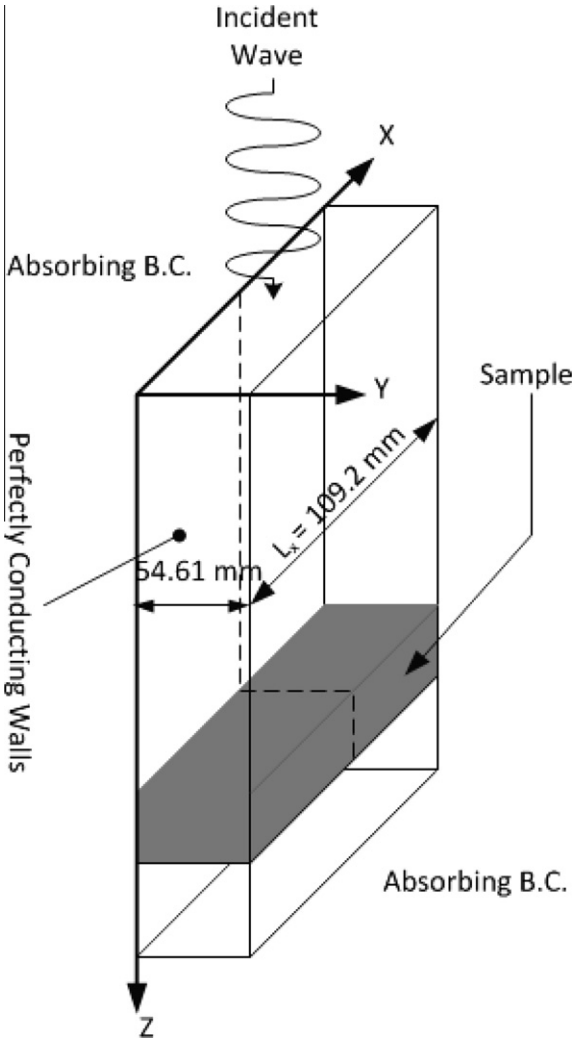

Fig. 3. Schematic of the physical problem.

Table 1
The electromagnetic and thermo physical properties used in the computations [4].

Material property	Air	Water	Glass bead	Alumina	Lead
Heat capacity, C_p ($Jg^{-1}\,K^{-1}$)	1.007	4.186	0.8	1.046	0.448
Thermal conductivity, λ ($W\,m^{-1}\,K^{-1}$)	0.0262	0.610	1.0	26.0	82.0
Density, ρ ($kg\,m^{-3}$)	1.205	1000	2500	3750	7660
Dielectric constant, ε_r'	1.0	$\varepsilon_r'(T)$[a]	5.1	10.8	6.9
Loss tangent, $\tan\delta$	0.0	$\tan\delta(T)$[b]	0.01	0.0145	0.0139

Note: For water, relative permittivity and loss tangent are referenced form Ratanadecho et al. [4] as follow:
[a] $\varepsilon_r'(T) = 85.56 - 0.3099T - 2.328x10^{-3}T^2 + 4.107x10^{-5}T^3 - 1.728x10^{-7}T^4$.
[b] $\tan\delta(T) = 0.2314 - 6.0405x10^{-3}T + 9.37x10^{-5}T^2 + 7.415x10^{-7}T^3 + 2.415x10^{-9}T^4$, T is in °C.

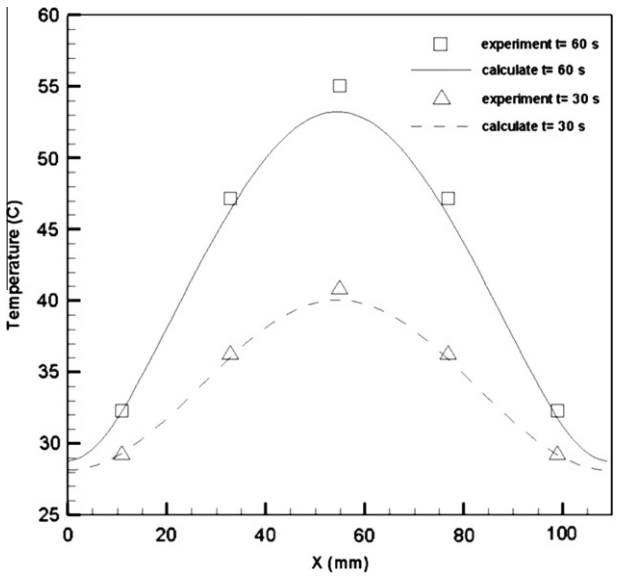

Fig. 4. The distributions of temperature for 30 and 60 s compared to the results from the calculations and experiment.

$$Z_H = \frac{\lambda_g Z_l}{\lambda} = \frac{\lambda_g}{\lambda}\sqrt{\frac{\mu}{\varepsilon}} \tag{17}$$

Here Z_l is the intrinsic impedance dependent on the properties of the material and λ and λ_g are the wave lengths of microwaves in free space and the rectangular wave guide, respectively.

The power flux associated with a propagating electromagnetic wave is expressed by the Poynting vector:

$$s = \frac{1}{2}\mathrm{Re}(E \times H^*) \tag{18}$$

The Poynting theorem allows the evaluation of the microwave power input, which is represented as:

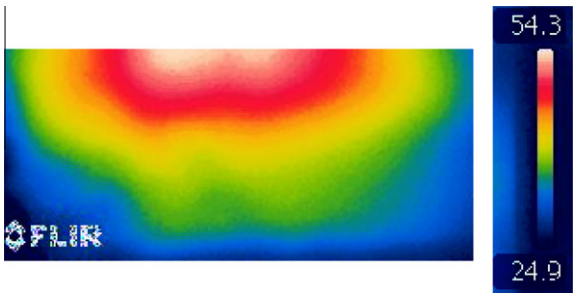

Fig. 5. Photograph taken from infrared camera shows contours of temperature (°C) in the porous packed bed at 60 s in case of porous two layers with glass beads with diameter of 0.15 mm at the top and 0.4 mm at the bottom.

$$P_{in} = \int_A SdA = \frac{A}{4Z_H}E_{yin}^2 \tag{19}$$

3.2. Analysis of temperature profile and flow field

The physical problem and coordinate system are depicted in Fig. 3. The microwave is propagating to the *xy* plane while the transport phenomena on the *xz* plane are currently investigated. To reduce the complexity of the problem, several assumptions have been offered into the flow and energy equations.

(1) Corresponding to the electromagnetic field, the flow and temperature fields can be assumed to be a two-dimensional plane.
(2) The effect of the phase change is neglected.
(3) Boussinesq approximation is used to account for the effect of the density variation on the buoyancy force.
(4) The surroundings of the porous packed bed are insulated except at the upper surface where energy exchanges with the ambient air.

3.2.1. Flow field equation

The porous medium is assumed to be homogeneous and thermally isotropic. The saturated fluid within the medium is in a local thermodynamic equilibrium (LTE) with the solid matrix [29–31]. The validity regime of local thermal equilibrium assumption has been established [32]. The fluid flow is unsteady, laminar and incompressible. The pressure work and viscous dissipation are all assumed to be negligible. The thermophysical properties of the

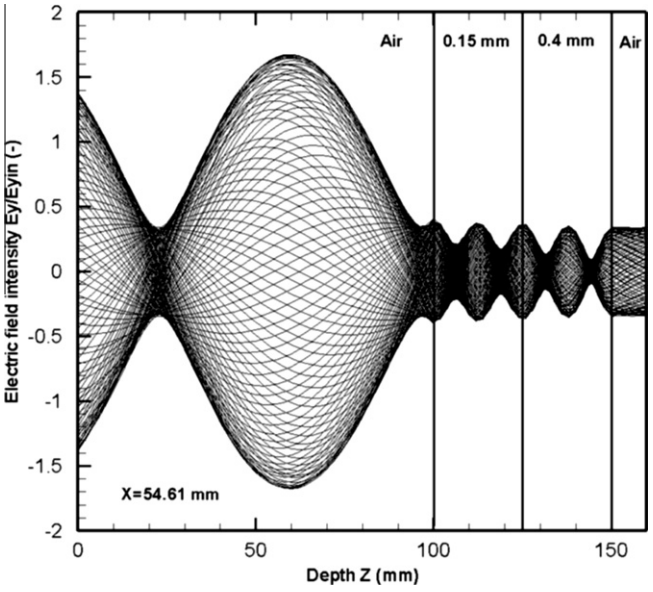

Fig. 6. Distribution of electric field on a porous two layers inside a rectangular waveguide at 60 s.

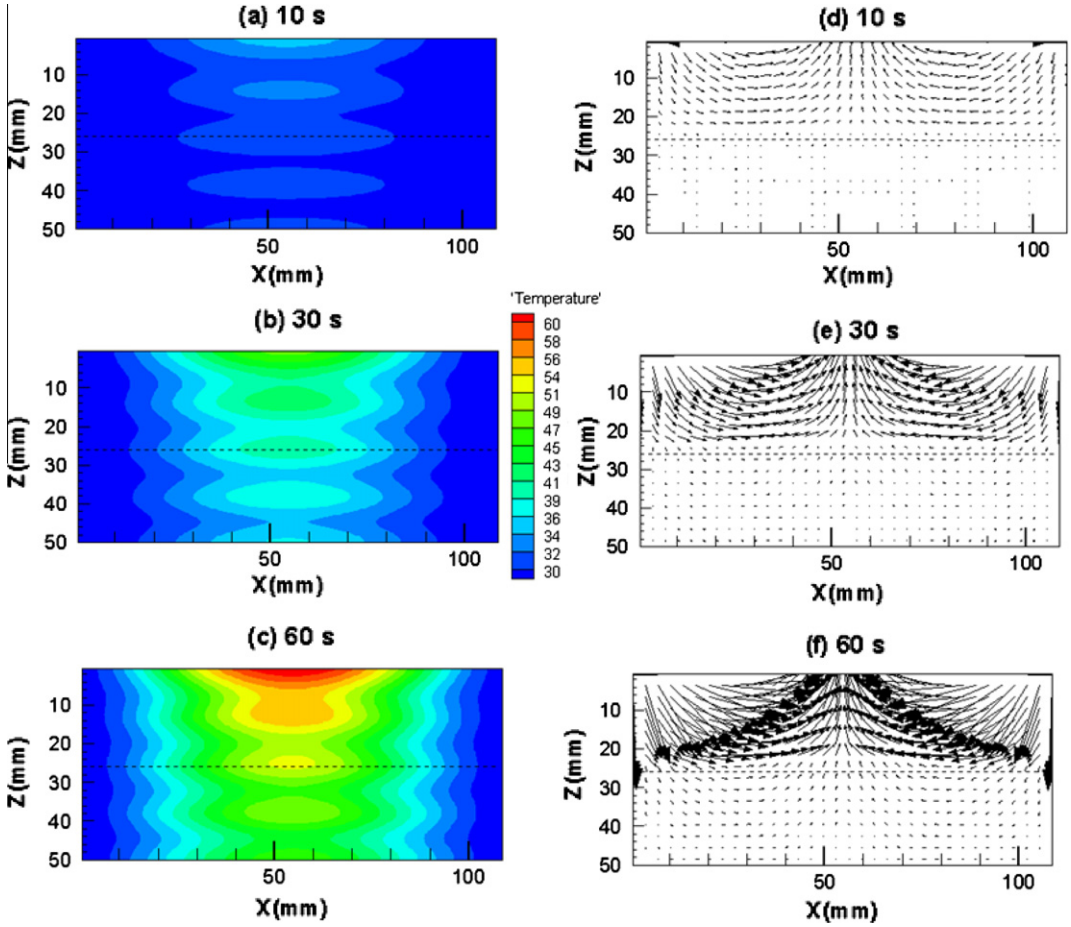

Fig. 7. Contours of temperature (°C) in the porous packed bed (a)–(c) and velocity vectors of water in porous materials, (d)–(f) at 10, 30, 60 s. Glass beads with diameter of 0.4 mm and 0.15 mm on the top and bottom layers, respectively. Both layers have a porosity of 0.385.

porous medium are taken to be constant however, the Boussinesq approximation takes into account of the effect of density variation on the buoyancy force. The Darcy–Forchheimer–Brinkman model was used to represent the fluid transport within the porous medium [32,33]. The Brinkmann's and the Forchheimer's extensions treats the viscous stresses at the bounding walls and the non-linear drag effect due to the solid matrix, respectively [33]. Furthermore, the solid matrix is made up of spherical particles, while the porosity and permeability of the medium are varied depending on the distance from the wall. Using standard symbols, the governing equations describing the heat transfer phenomenon are given by

Continuity equation:

$$\frac{\partial u}{\partial x}+\frac{\partial w}{\partial z}=0 \tag{20}$$

Momentum equations:

$$\frac{1}{\phi}\frac{\partial u}{\partial t}+\frac{u}{\phi^2}\frac{\partial u}{\partial x}+\frac{w}{\phi^2}\frac{\partial u}{\partial z}=-\frac{1}{\rho_f}\frac{\partial p}{\partial x}+\frac{\upsilon}{\phi}\left(\frac{\partial^2 u}{\partial x^2}+\frac{\partial^2 u}{\partial z^2}\right)-\frac{\mu u}{\rho_f \kappa}-F(u^2+w^2)^{1/2} \tag{21}$$

$$\frac{1}{\phi}\frac{\partial w}{\partial t}+\frac{u}{\phi^2}\frac{\partial w}{\partial x}+\frac{w}{\phi^2}\frac{\partial w}{\partial z}=-\frac{1}{\rho_f}\frac{\partial p}{\partial z}+\frac{\upsilon}{\phi}\left(\frac{\partial^2 w}{\partial x^2}+\frac{\partial^2 w}{\partial z^2}\right)-\frac{w\mu}{\rho_f \kappa}-F(u^2+w^2)^{1/2}+g\beta(T-T_0) \tag{22}$$

where ϕ, v and β are porosity, kinematics viscosity and coefficient of thermal expansion of the water layer, respectively. The permeability κ and geometric F function are [17,34]

$$\kappa=\frac{d_p^2\phi^3}{175(1-\phi)^2} \tag{23}$$

$$F=\frac{1.75(1-\phi)}{d_p\phi^3} \tag{24}$$

The porosity is assumed to vary exponentially with the distance from the wall [14,16,22]. Based on these previous studies, we proposed the variation of porosity within three confined walls of the bed; a bottom wall and two lateral walls. The expression that considers the variation of porosity in two directions in the xz plane is given by

$$\phi=\phi_s\left[1+b\left\{exp\left(-\frac{bx}{dp}\right)+exp\left(-\frac{b(W-x)}{dp}\right)+exp\left(-\frac{bz}{dp}\right)\right\}\right] \tag{25}$$

where d_p is the diameter of glass beads, ϕ_s known as the free-stream porosity is the porosity far away from the walls, W is the width of the packed bed and b and c are empirical constants. The dependencies of b and c to the ratio of the bed to bead diameter is small, and b and c were suggested to be 0.98 and 1.0, respectively [15].

3.2.2. Heat transfer equation

The temperature of the liquid layer exposed to the incident wave is obtained by solving the conventional heat transport equation with the microwave power absorbed included as a local electromagnetic heat generation term:

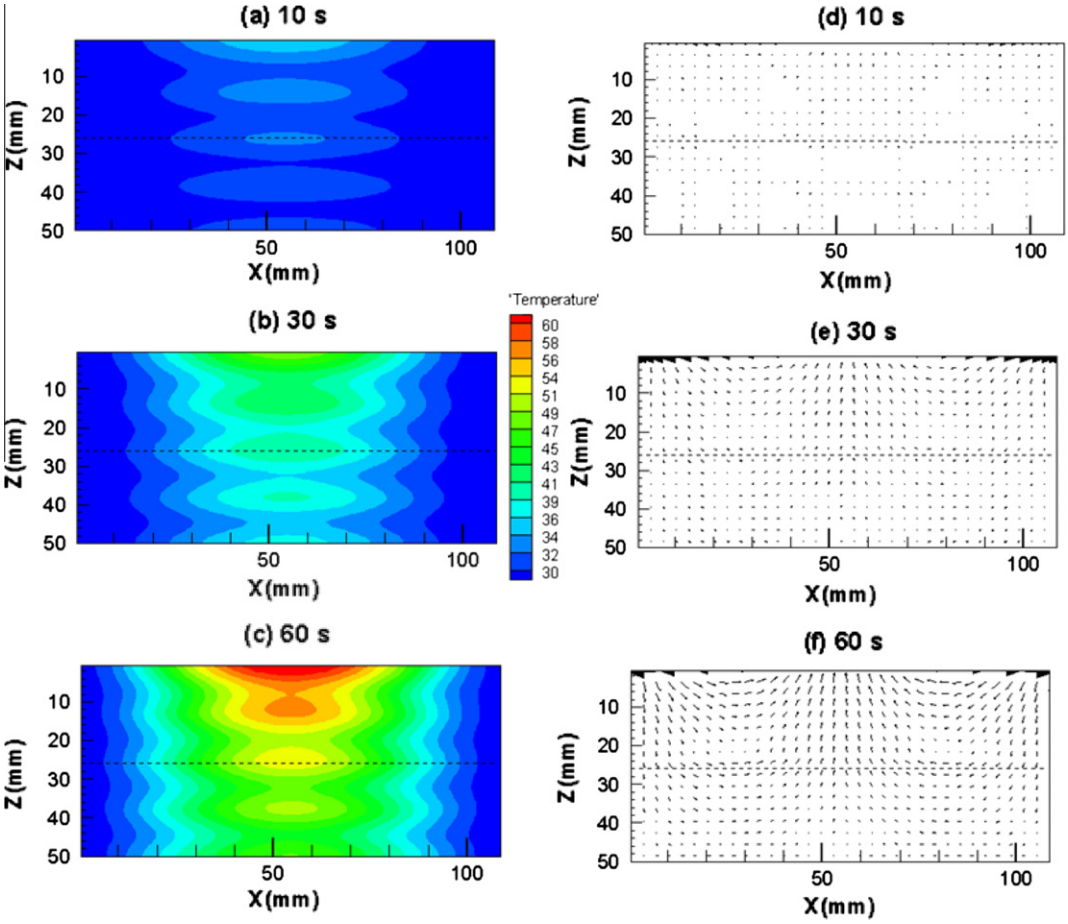

Fig. 8. Contours of temperature (°C) in the porous packed bed (a)–(c) and velocity vectors of water in porous materials, (d)–(f) at 10, 30, 60 s. Glass beads with diameter of 0.15 mm and 0.4 mm on the top and bottom layers, respectively. Both layers have a porosity of 0.385.

$$\sigma\frac{\partial T}{\partial t}+u\frac{\partial T}{\partial x}+w\frac{\partial T}{\partial z}=\alpha\left(\frac{\partial^2 T}{\partial x^2}+\frac{\partial^2 T}{\partial z^2}\right)+Q \tag{26}$$

where specific heat ratio $\sigma=\frac{[\phi(\rho c_p)_f+(1-\varepsilon)(\rho c_p)_s]}{(\rho c_p)_f}$, $\alpha=k_e/(\rho c_p)_f$ is the thermal diffusivity.

The local electromagnetic heat generation term that is a function of the electric field and is defined as

$$Q=2\pi f\varepsilon_0\varepsilon_r'\tan\delta(E_y)^2 \tag{27}$$

Boundary and initial conditions for these equations:

Since the walls of the container are rigid, the velocities are zero. At the interface between the porous layers and the walls of the container, zero slip boundary conditions are used for the momentum equations.

(1) At the upper surface, the velocity in the normal direction (w) and shear stress in the horizontal direction are assumed to be zero, where the influence of Marangoni flow [7] can be applied:

$$\eta\frac{\partial u}{\partial z}=-\frac{d\xi}{dT}\frac{\partial T}{\partial x} \tag{28}$$

(2) The walls, except the top wall, are insulated so no heat or mass exchanges:

$$\frac{\partial T}{\partial x}=\frac{\partial T}{\partial z}=0 \tag{29}$$

(3) Heat is lost from the surface via natural convection and radiation:

$$-k_{eff}\frac{\partial T}{\partial z}=h_c(T-T_0) \tag{30}$$

where

$$k_{eff}=\varepsilon k_f+(1-\varepsilon)k_s \tag{31}$$

(4) The interface boundary condition between layer 1st and layer 2nd are given by:

$$k_{eff}\frac{\partial T_1}{\partial y}=k_{eff}\frac{\partial T_2}{\partial y},\quad T_1=T_2 \tag{32}$$

$$\mu\left.\frac{du}{dy}\right|_1=\mu\left.\frac{du}{dy}\right|_2,\quad u_1=u_2,\quad v_1=v_2 \tag{33}$$

These conditions have been utilized at the interface between two different porous media with reasonably accurate results [35–36].

(5) The initial condition of a medium is defined as:

$$T=T_0\quad \text{at } t=0 \tag{34}$$

When T_0 is initial temperature at 28 °C.

4. Numerical procedure

The description of heat transport and flow pattern of liquid layer eqs. 20, 21, 22, 23, 24 and (26) require specification of temperature (T), velocity components (u,w) and pressure (p). These equations are coupled to the Maxwell's equations (Eqs. (1)–(3)) by Eq. (27), which represents the heating effect of the microwaves in the liquid-container domain.

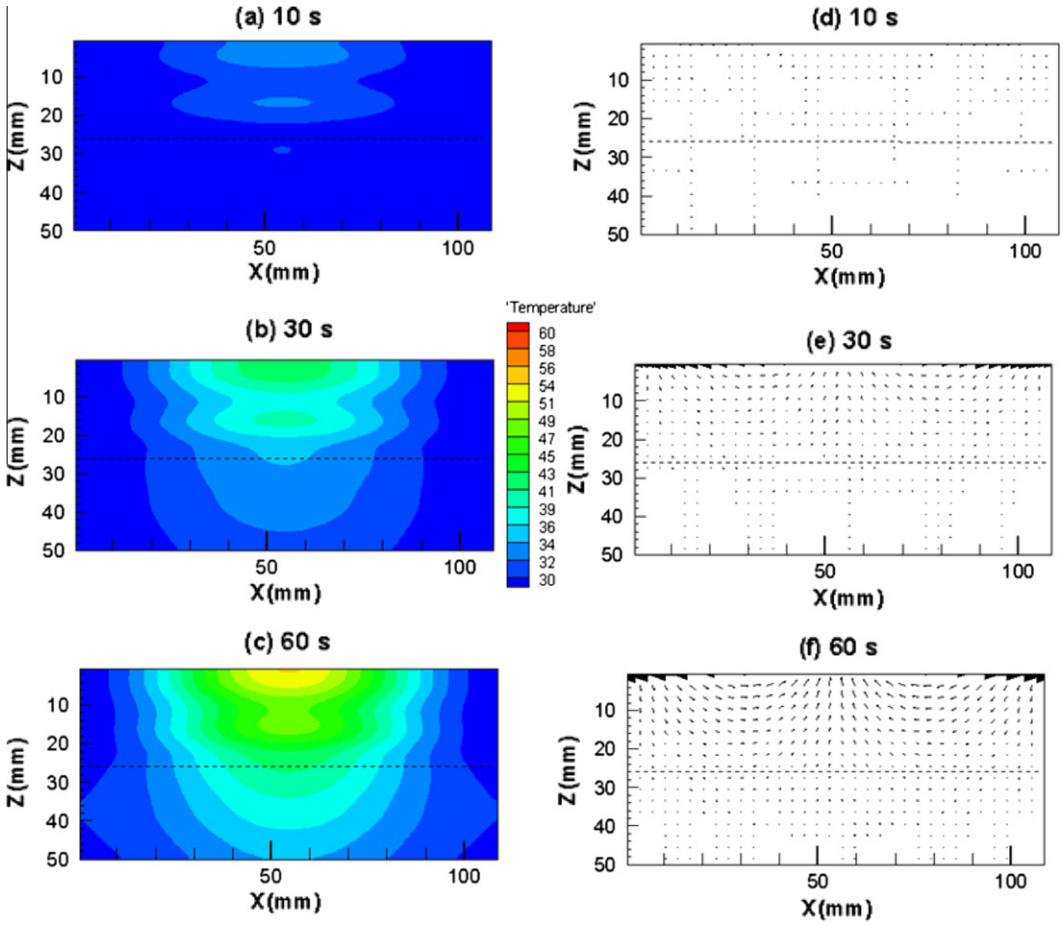

Fig. 9. Contours of temperature (°C) in the porous packed bed (a) (c) and velocity vectors of water in porous materials, (d) (f) at 10, 30, 60 s. Glass beads are on top and alumina balls are in the bottom, both layers have diameter and porosity equal to 0.15 mm and 0.385, respectively.

4.1. Electromagnetic equations and FDTD discretization

The electromagnetic equations are solved by using the finite difference time domain (FDTD) method that provides detailed spatial and temporal information of electromagnetic wave propagation. With this method the electric field components (E) are stored halfway between the basic nodes while magnetic field components (H) are stored at the center. Thus they are calculated at alternating half-time steps. E and H field components are discretized by a central difference method (second-order accurate) in both spatial and time domain. The leapfrog scheme is utilized for time integrations of the Maxwell's equations until the steady-state electromagnetic field behavior is fully evolved.

4.2. Fluid flow and heat transport equations and finite control volume discretization

Eqs. (20)–(24) are solved numerically by using the finite control volume along with the SIMPLE algorithm developed by Patankar [37]. The reason for using this method is the advantage provided from flux conservation that avoids the generation of a parasitic source. The basic strategy of the finite control volume discretization method is to divide the calculated domain into a number of control volumes and then integrate the conservation equations over this control volume and over an interval of time[$\{t, t + \Delta t\}$]. At the boundaries of the calculated domain, the conservation equations are discretized by integrating over half the control volume, taking into account the boundary conditions. At the corners of the calculated domain we used a quarter of the control volume. The fully Euler implicit time discretization finite difference scheme is used to arrive at the solution in time.

4.2.1. The stability and accuracy of calculation

The choice of spatial and temporal resolution is motivated by reasons of stability and accuracy. To ensure stability of the time stepping algorithm, Δt must be chosen to satisfy the courant stability condition and is defined as

$$\Delta t \leqslant \frac{\sqrt{(\Delta x)^2 + (\Delta z)^2}}{\upsilon} \tag{35}$$

and the spatial resolution of each cell is defined as

$$\Delta x, \Delta z \leqslant \frac{\lambda_g}{10\sqrt{\varepsilon_r}} \tag{36}$$

Corresponding to Eqs. (32) and (33) the calculation conditions are as follows:

(1) Grid resolution is 100 (x) × 200 (z).
(2) Grid size: $\Delta x = 1.0922$ mm and $\Delta z = 1.0000$ mm
(3) Time steps: $\Delta t = 2 \times 10^{-12}$ s and $\Delta t = 0.005$ s are used corresponding to the electromagnetic field and temperature field calculations, respectively.
(4) Relative error in the iteration procedures of 10^{-6} was chosen.

The mesh of 100 × 200 was found to be sufficient for the simulations carried out in the present study. Independence of the solutions on the grid size was examined through a number of test

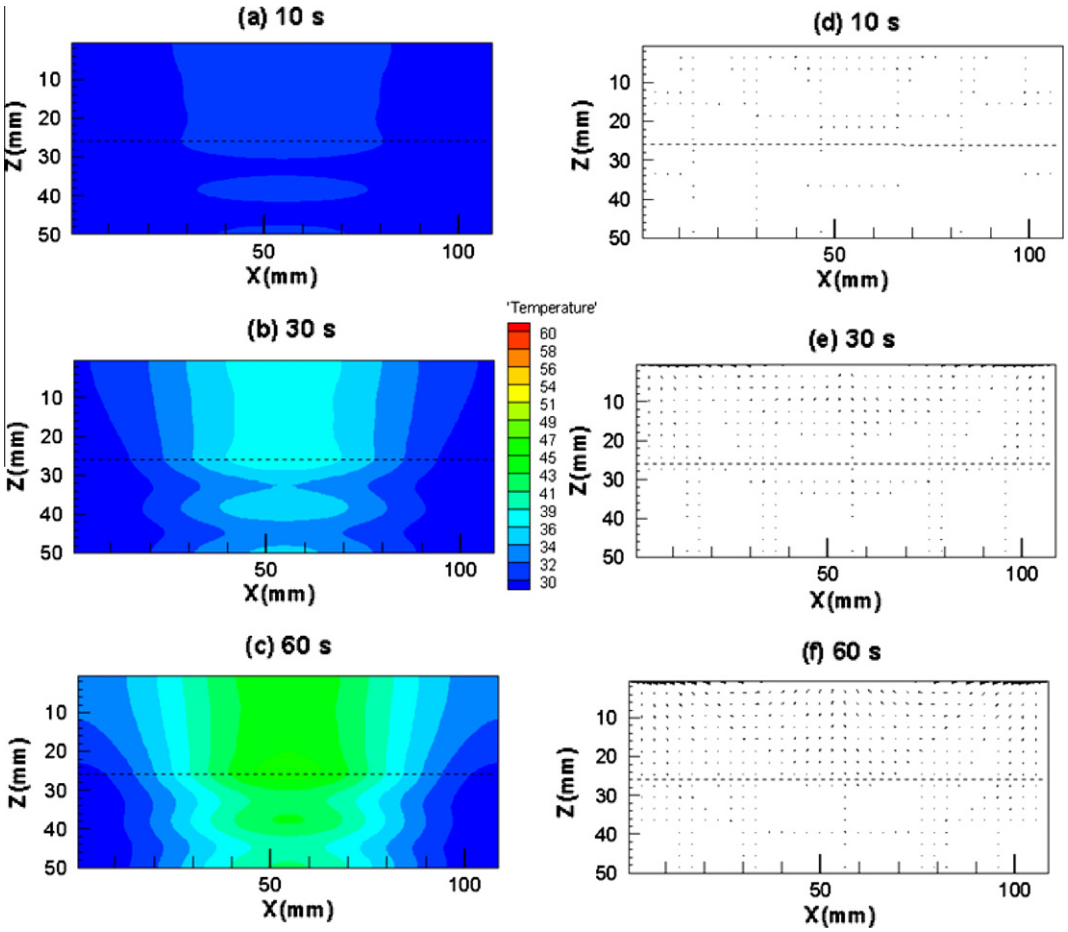

Fig. 10. Contours of temperature (°C) in the porous packed bed (a)–(c) and velocity vectors of water in porous materials, (d)–(f) at 10, 30, 60 s. Alumina balls are on top and Glass beads are in the bottom, both layers have diameter and porosity equal to 0.15 mm and 0.385, respectively.

cases. The results indicate that negligible difference of solutions was achieved above the resolution of 80 × 160 [7].

4.2.2. The iterative computational schemes

Since the dielectric properties of liquid layer samples are temperature dependent, to understand the influence of the electromagnetic fields on the microwave heating of a liquid layer it is necessary to consider the coupling between electric field and temperature and fluid flow fields. For this reason, iterative computational schemes are required to resolve the coupled non-linear Maxwell's equations, momentum and heat transport equations.

The computational scheme is to first computes a local heat generation term by running an electromagnetic calculation with uniform properties determined from initial temperature data. The electromagnetic calculation is performed until a sufficient period is reached in which the representative average rms (root mean square) of the electric field at each point is computed and used to solve the time dependent temperature and velocities field. Using these temperatures new values of the dielectric properties are calculated and used to re-calculate the electromagnetic fields and then the microwave power absorption. All the steps are repeated until the required heating time is reached.

5. Results and discussion

The numerical results are compared against the experimental data. The present analysis involves several types of materials. The dielectric and thermal properties of air, water, glass bead, alumina and lead used for computations are listed in Table 1. The two layered porous medium is composed of smaller glass beads on top of bigger beads with 0.15 mm and 0.4 mm in diameter, respectively. The comparison is shown in Fig. 4 for the temperature distributions in *XZ* plane at the horizontal line $Z = 20$ mm at 30 s and 60 s. The results reveal good agreement between the computations and measurement. It is found that the difference is less than 3.3%. The favorable comparisons lend confidence to accuracy of the present model and further numerical studies herein.

Fig. 5 is a photograph taken by the infrared camera that shows the contour of the temperature (°C) at the *x*–*z* plane surface in the case of a two layers porous medium. This photograph shows glass beads in the packed bed that is 50 mm high, the glass beads 0.15 mm in diameter are placed on top of the bigger glass beads 0.4 mm in diameter. It is observed that temperature is greatest at the top of photograph at about 54 °C. From the photograph we found that the distribution of temperature due to heating by microwave will be similar in many experiments. The temperature contour taken from the camera is consistent with the results given in Fig. 4.

For a better understanding of the electric field inside the rectangular waveguide containing a porous packed bed, an electric field in TE_{10} mode at the center of *x* at 54.61 mm of the rectangular waveguide is extracted and shown in Fig. 6. The sample inside the waveguide is the water saturated packed bed filled with 0.15 mm diameter glass beads on top of 0.4 mm diameter beads. The vertical axis denotes the ratio of the intensity of the electric

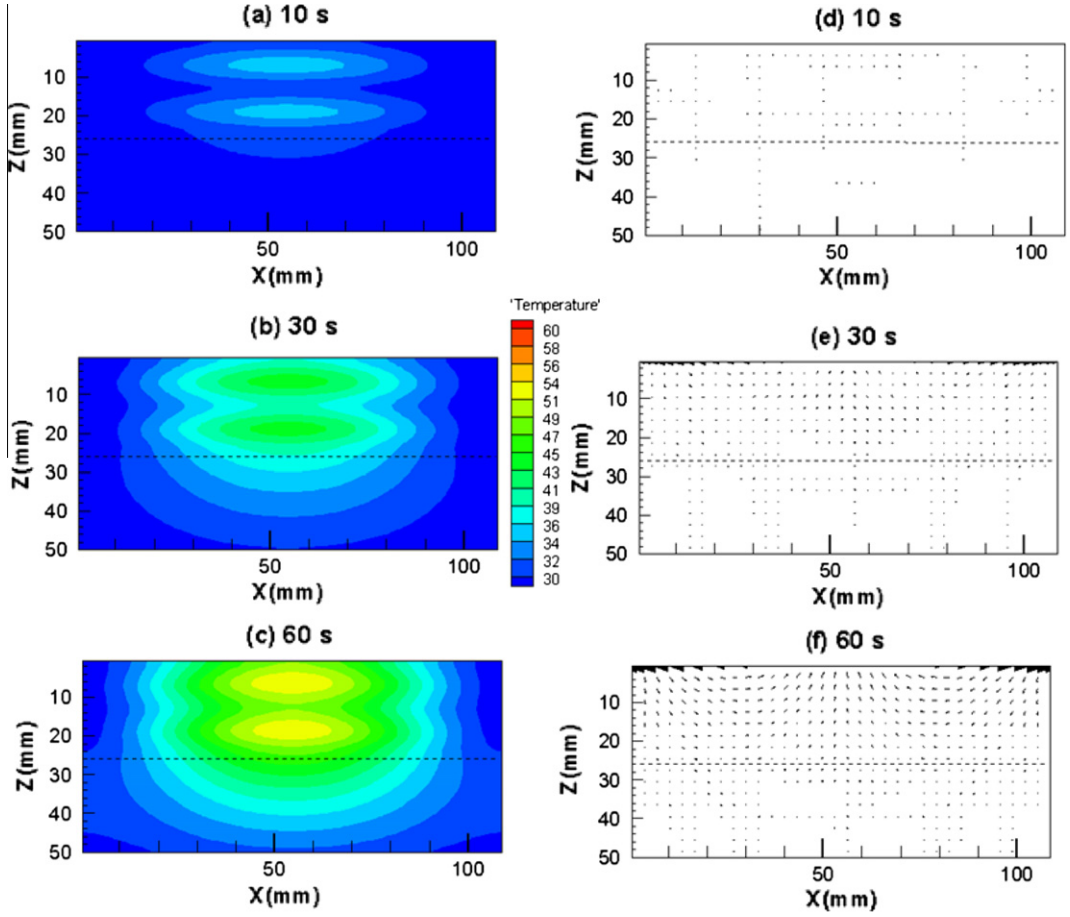

Fig. 11. Contours of temperature (°C) in the porous packed bed (a)–(c) and velocity vectors of water in porous materials, (d)–(f) at 10, 30, 60 s. Glass beads are on top and lead balls are in the bottom, both layers have diameter and porosity equal to 0.15 mm and 0.385, respectively.

field (E_y) and input electric field (E_{yin}). Since the waves transmitted through the cavity with air inside which low relative permittivity travel to the sample has high relative permittivity. Most of the waves are reflected from the surface of the sample occur interference with waves that forward so in front of sample. This phenomenon is called resonance of standing wave that occurs at the empty part waveguide (left side of the example). The amplitude of the wave is increased while the amplitude of the electric field inside the material is reduced due to the microwave energy that is lost into thermal energy. However, distributions of the electric field in this case produce a standing wave in front of porous material are mainly caused by part of water in the porous media. Electrical conductivity and relative permittivity strongly affect formation of standing waves.

Next, effects of particle size and patterns of layers are investigated. Figs. 7 and 8 are numerical results of two-layer porous media compared of glass beads. The two layers have different sizes of glass beads. In Fig. 7, glass beads with diameter of 0.4 mm are filled in the top layers while glass beads with a diameter of 0.15 mm are in the bottom layer. The boundary between layers is at the $Z = 25$ mm. In Fig. 8, the two layers swap over. In both Figs. 7 and 8, porosity is 0.38 for the entire domain and the microwave power of 300 watts is used. It can be seen that, in case of the coarse beads (0.4 mm) on top (Fig. 7) the rate of heat transfer is slower than the case that fine beads (0.15 mm) are on the top (Fig. 8). This result is due to the coarse beads on top that have higher permeability making fluid to flow faster than the bottom layer that contains fine beads. Most of the fluid mass reflects at the interface since it is difficult for fluid to flow through the fine beads that have low permeability. For this reason, the heat transfer within the fine beads is less efficiency.

In order to analyze effects of material properties on heating processes in double layer medium, the two layer porous medium with glass beads and alumina balls is tested. Fig. 9 is the computed results for the case that glass beads are on top of alumina balls. The positions of materials are switched in Fig. 10. Glass beads and alumina balls have different relative dielectric constants 5.1 and 10.8, respectively. Thermal conductivity of the glass beads and alumina balls are 1.0 W/(m K) and 26.0 W/(m K), respectively. The calculated result in Fig. 10 shows that the thermal distribution is wider and its gradients are smaller with lower temperature, compared to Fig. 9. Since alumina in the upper layer has thermal conductivity 26 times greater than glass. High value of thermal conductivity enhances heat transfer rate. In addition, higher relative dielectric constant of alumina indicates less heat absorption in the upper layer. Due to the fact that the penetration depth of the glass beads is greater than the thickness of the layer of glass beads approximately two times, the standing wave or resonance occurs from a combination of forward and reflected waves at the boundary between the glass bead and alumina layers.

Fig. 11 is the calculated domain for which glass beads on top and lead balls in the bottom. Locations of the two layers are switched and shown in Fig. 12. Both of the layers reveal different profiles since their thermal conductivities differ by 82 times. Glass and lead have the thermal conductivity of 1 W/(m K) and 82.0 W/(m K), respectively. It can be noticed that the temperature contour

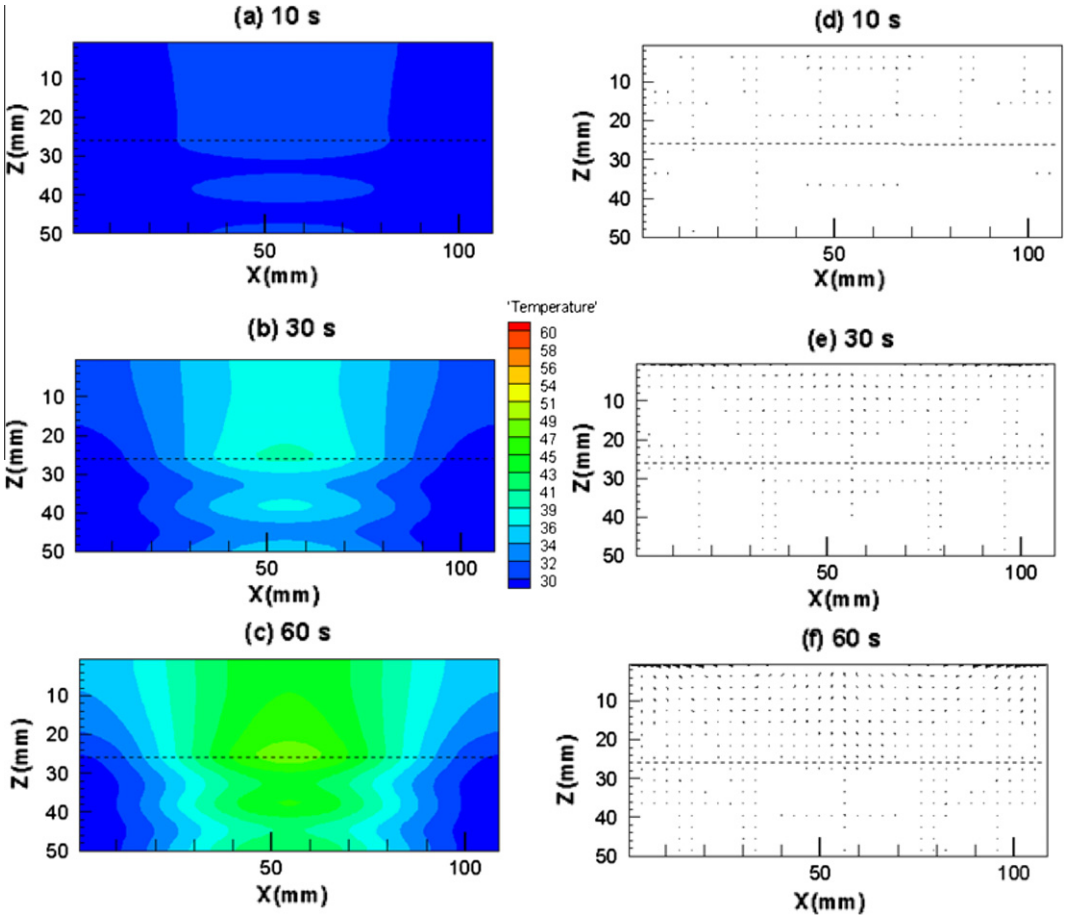

Fig. 12. Contours of temperature (°C) in the porous packed bed (a)–(c) and velocity vectors of water in porous materials, (d)–(f) at 10, 30, 60 s. Lead balls are on top and Glass beads are in the bottom, both layers have diameter and porosity equal to 0.15 mm and 0.385, respectively.

patterns in the Figs. 11 and 12 are similar to Figs. 9 and 10, respectively. However, in the case of lead, the contour spreads more widely since lead has much greater thermal conductivity than alumina. Besides, lead has a dielectric constant less than alumina. Electric wave can be stored into the lead layer more than alumina. When focusing on the top layers which both are filled with glass beads in Figs. 9 and 11, patterns of wave resonance are different within the layers. This result is attributed to the difference of material type in the bottom layer. Lead layer at bottom causes reflected wave as clearly seen in the Figure more than when the bottom material is alumina. Therefore thermal and dielectric properties of material in the bottom layer markedly affect the heating process within the top layer.

6. Conclusions

Heating process in the double-layer porous media subjected to microwave energy is numerically investigated. Effects of particle size thermal and dielectric properties of the media are examined.The porous packed bed as the medium was placed in a waveguide with a rectangular cross section. The two layers have different materials or different particle sizes. The microwave power of 300 W and frequency of 2.45 GHz in TE_{10} mode were used. The calculations based on the mathematical model are consistent with the results of experiment. The major results found are as follows. Regarding fine and course beads, heating rate is higher when fine beads is on top due to the enhanced convective flow in porous materials. Different materials between two layers affect the reflection of waves at the interface. Due to the difference in dielectric properties of materials standing wave are produced in the upper layer, resulting in higher rates of heat transfer within the upper layer. Heat transfer is less efficient when porous material on the top layer has high relative dielectric constant since less electric waves are not absorbed in the material. On the other hand, heat spreads faster in materials with higher thermal conductivity. Finally, heating processes within the top layer are remarkably affected by the thermal and dielectric properties of material in the bottom layer.

References

[1] W.K. Chen, H.T. Davis, E.A. Davis, G. Joan, Heat and mass transfer in water-laden sandstone microwave heating, AIChE J. 31 (5) (1985) 842–848.
[2] H. Ni, A.K. Datta, K.E. Torrance, Moisture transport in intensive microwave heating of biomaterials: porous media model, Int. J. Heat Mass Transfer 42 (1999) 1501–1512.
[3] H. Feng, J. Tang, R.P. Cavalieri, O.A. Plumb, Heat and mass transport in microwave drying of porous materials in a spouted bed, AIChE J. 47 (2001) 1499–1512.
[4] P. Ratanadecho, K. Aoki, M. Akahori, Influence of irradiation time particle sizes and initial moisture content during microwave drying of multi-layered capillary porous materials, ASME J. Heat Transfer 124 (1) (2002) 151–161.
[5] D.D. Dincov, K.A. Parrot, K.A. Pericleous, Heat and mass transfer in two- phase porous materials under intensive microwave heating, J. Food Eng. 65 (2006) 403–412.
[6] P. Ratanadecho, The simulation of microwave heating of wood using a rectangular wave guide: influence of frequency and sample size, Chem. Eng. Sci. (61) (2006) 4798–4811.
[7] P. Ratanadecho, K. Aoki, M. Akahori, A numerical and experimental investigation of modelling of microwave heating for liquid layers using a rectangular wave guide (effects of natural convection and dielectric properties), Appl. Math. Model. 26 (2002) 449–472.

[8] W. Cha-um, P. Rattanadecho, W. Pakdee, Experimental analysis of microwave heating of dielectric materials using a rectangular wave guide (MODE: TE10) (case study: water layer and saturated porous medium), Exp. Therm. Fluid Sci. 33 (3) (2009) 472–481.
[9] K.G. Ayappa, S. Brandon, Microwave driven convection in a square cavity, AIChE J. 40 (7) (1994) 1268–1272.
[10] A.S. Franca, K. Haghighi, Adaptive finite element analysis of microwave driven convection, Int. Commun. Heat Mass Transfer 23 (2) (1996) 177–186.
[11] S. Chatterjee, T. Basak, S.K. Das, Microwave driven convection in a rotating cylindrical cavity: a numerical study, J. Food Eng. 79 (2007) 1269–1279.
[12] A.L. Brody, Advances in microwave pasteurization and sterilization, Food Technol. 65 (2) (2011) 83–85.
[13] S. Lui, J. Masliyah, Single fluid flow in porous media, Chem. Eng. Commun. 148 (1996) 653–732.
[14] R.F. Benenati, C.B. Brosilow, Void fraction distribution in pack beds, AIChE J. 8 (1962) 359–361.
[15] K. Vafai, Convective flow and heat transfer in variable-porosity media, J. Fluid Mech. 147 (1984) 233–259.
[16] A. Amiri, K. Vafai, Analysis of dispersion effects and non-thermal equilibrium, non-Darcian, variable porosity incompressible flow through porous media, Int. J. Heat Mass Transfer 37 (6) (1994) 939–954.
[17] A.K. Abdul-Rahim, A.J. Chamkha, Variable porosity and thermal dispersion effects on coupled heat and mass transfer by natural convection from a surface embedded in a non-metallic porous medium, Int. J. Numer. Methods Heat Fluid Flow 11 (5) (2001) 413–429.
[18] S.W. Hsiao, P. Cheng, C.K. Chen, Non-uniform porosity and thermal dispersion effects on natural convection about a heated horizontal cylinder in an enclosed porous medium, Int. J. Heat Mass Transfer 35 (12) (1992) 3407–3418.
[19] H. Sakamoto, F.A. Kulacki, Effective thermal diffusivity of porous media in the wall vicinity, ASME J. Heat Transfer 130 (2) (2008). art.no. 022601.
[20] K. Vafai, Analysis of the channeling effect in variable porosity media, J. Energy Resour. Technol. 108 (1986) 131–139.
[21] M.L. Hunt, C.L. Tien, Non-Darcian convection in cylindrical packed beds, ASME J. Heat Transfer 110 (1998) 2523–2532.
[22] D. Poulikakos, K. Renken, Forced convection in a channel filled with porous medium, including the effects of flow inertia, variable porosity and Brinkman friction, ASME J. Heat Transfer 109 (1987) 880–888.
[23] H. Shih-Wen, P. Cheng, C. Chao-Kuang, Non-uniform porosity and thermal dispersion effects on natural convection about a heated horizontal cylinder in an enclosed porous medium, Int. J. Heat Mass Transfer 35 (12) (1992) 3407–3418.
[24] Z. Chai, Z. Guo, Study of electro-osmotic flows in microchannels packed with variable porosity media via lattice Boltzmann method, J. Appl. Phys. 101 (2007) 104913.
[25] S. Akbal, F. Baytas, Effects of non-uniform porosity on double diffusive natural convection in a porous cavity with partially permeable wall, Int. J. Therm. Sci. 47 (7) (2008) 875–885.
[26] R. Prommas, P. Kengin, P. Rattanadecho, Energy and exergy analyses in convective drying process of multi-layered porous packed bed, Int. Commun. Heat Mass Transfer 37 (2010) 1106–1114.
[27] W. Pakdee, P. Rattanadecho, Natural convection in a saturated variable-porosity medium due to microwave heating, ASME J. Heat Transfer 133 (6) (2011). art. no. 062502.
[28] W. Klinbun, K. Vafai, P. Rattanadecho, Electromagnetic field effects on transport through porous media, Int. J. Heat Mass Transfer 55 (2012) 325–335.
[29] M.M. El-Refaee, M.M. Elsayed, N.M. Al-Najem, A.A. Noor, Natural convection in partially cooled tilted cavities, Int. J. Numer. Methods Heat Fluid Flow 28 (1998) 477–499.
[30] D.A. Nield, A. Bejan, Convection in Porous Media, Springer, New York, 1999.
[31] A.A. Al-Amiri, Natural convection in porous enclosures: the application of the two-energy equation model, Numer. Heat Transfer Part A 411999 (2002) 817–834.
[32] A. Marafie, K. Vafai, Analysis of non-Darcian effects on temperature differentials in porous media, Int. J. Heat Mass Transfer 44 (2001) 4401–4411.
[33] P. Nithiarasu, K.N. Seetharamu, T. Sundararajan, Natural convective heat transfer in a fluid saturated variable porosity medium, Int. J. Heat Mass Transfer 40 (1996) 3955–3967.
[34] A.J. Chamkha, C. Issa, K. Khanafer, Natural convection from an inclined plate embedded in a variable porosity porous medium due to solar radiation, Int. J. Therm. Sci. 41 (2001) 73–81.
[35] K. Vafai, R. Thiyagaraja, Analysis of flow and heat transfer at the interface region of a porous medium, Int. J. Heat Mass Transfer 30 (1987) 1391–1405.
[36] S.J. Kim, C.Y. Choi, Convection heat transfer in porous and overlaying layers heated from below, Int. J. Heat Mass Transfer 39 (1996) 319–329.
[37] S.V. Patankar, Numerical Heat Transfer and Fluid Flow, Hemisphere, New York, 1980.